Mon. Not. R. Astron. Soc. **402,** 941–955 (2010) doi:10.1111/j.1365-2966.2009.15945.x

# Two phase galaxy formation: the gas content of normal galaxies

M. Cook,[1,2⋆] C. Evoli,[1] E. Barausse,[1,3] G. L. Granato[2,4] and A. Lapi[1,4,5]

[1]*Astrophysics Sector, SISSA/ISAS, Via Beirut 2-4, I-34151 Trieste, Italy*
[2]*INAF, Osservatorio Astronomico di Padova, Vicolo dell' Osservatorio 5, I-35122 Padova, Italy*
[3]*Centre for Fundamental Physics, University of Maryland, College Park, MD 20742-4111, USA*
[4]*INAF, Osservatorio Astronomico di Trieste, Via G.B. Tiepolo 11, I-34131 Trieste, Italy*
[5]*Department of Physics, Univ. di Roma 'Tor Vergata', Via della Ricerca Scientifica 1, I-00133 Rome, Italy*

Accepted 2009 October 22. Received 2009 October 22; in original form 2009 June 22

**ABSTRACT**

We investigate the atomic (H I) and molecular ($H_2$) Hydrogen content of normal galaxies by combining observational studies linking galaxy stellar and gas budgets to their host dark matter (DM) properties, with a physically grounded galaxy formation model. This enables us to analyse empirical relationships between the virial, stellar and gaseous masses of galaxies, and explore their physical origins. Utilizing a semi-analytic model (SAM) to study the evolution of baryonic material within evolving DM haloes, we study the effects of baryonic infall and various star formation and feedback mechanisms on the properties of formed galaxies using the most up-to-date physical recipes. We find that in order to significantly improve the agreement with observations of low-mass galaxies, we must suppress the infall of baryonic material and exploit a two-phase interstellar medium, where the ratio of H I to $H_2$ is determined by the galactic disc structure. Modifying the standard Schmidt–Kennicutt star formation law, which acts upon the total cold gas in galaxy discs and includes a critical density threshold, and employing a star formation law which correlates with the $H_2$ gas mass results in a lower overall star formation rate. This, in turn, allows us to simultaneously reproduce stellar, H I and $H_2$ mass functions of normal galaxies.

**Key words:** galaxies: evolution – galaxies: formation – cosmology: theory – dark matter.

## 1 INTRODUCTION

Neutral atomic hydrogen is the most abundant element in the Universe and plays a fundamental role in galaxy formation, principally as the raw material from which stars form. Within galaxies, the interstellar medium (ISM) acts as a temporally evolving baryonic component; competing processes cause the accumulation (through external infall from the intergalactic medium and stellar evolution) and depletion (through star formation and various feedback mechanisms) of hydrogen. Thus, observational determinations and theoretical predictions of the hydrogen budget within galaxies of various masses and morphologies are of central importance to constraining the physics of galaxy formation (see Kauffmann, White & Guilderoni 1993; Benson et al. 2003; Yang, Mo & van den Bosch 2003; Mo et al. 2005; Kaufmann et al. 2009)

Moreover, within the ISM hydrogen comprises the majority of the cold gas mass, and when non-ionized exists within two-phases, atomic H I and molecular $H_2$. A large body of observational analysis has shown that within galaxies, H I generally follows a smooth, diffuse distribution whereas $H_2$ regions are typically dense, optically thick clouds which act as the birthplaces for newly formed stars (Drapatz & Zinnecker 1984; Wong & Blitz 2002; Blitz & Rosolowski 2004; Krumholz & McKee 2005; Wu et al. 2005; Blitz & Rosolowsky 2006). Due to the distinct differences in these phases, and the central importance of ISM physics to the evolution of galaxies, cosmological simulations have begun to include both phases (see Gnedin, Tassis & Kravstov 2009 and references therein), and observations have begun focusing on simultaneous measurements of both H I and $H_2$ (see Obreschkow & Rawlings 2009).

The distinction between these two phases has recently been shown to be of crucial importance to constrain the physics of galaxy formation. In particular, resolved spectroscopy using Galaxy Evolution Explorer (GALEX) showing obscured star-forming regions in nearby galaxies (Kennicutt et al. 2003, 2007; Calzetti et al. 2007; Gil de Paz et al. 2007), and various observational surveys providing maps of gas in galaxies at high-resolutions (Helfer et al. 2003; Walter et al. 2008; Leroy et al. 2009), have revealed a deeper level of complexity on subgalactic scales. These studies allowed theoretical models for the ISM and star formation to be constrained and further developed.

Furthermore, due to the constant replenishment and depletion of hydrogen in either H I or $H_2$ phases, and to their separate yet interlinked properties, at any epoch, measurements of the fraction of H I

⋆E-mail: cook@sissa.it

and $H_2$ are highly constraining for the processes of molecular cloud formation, star formation, baryonic infall and various feedbacks. Therefore, simultaneously predicting the stellar and gas mass functions of normal galaxies is a major challenge for any physically motivated galaxy formation model, requiring an accurate depiction of all of the aforementioned processes (see Mo et al. 2005 for a detailed discussion). These issues manifest most clearly within the largely successful $\Lambda$ cold dark matter ($\Lambda$CDM) paradigm within the lowest mass systems, where it still remains unclear whether strongly non-linear feedback mechanisms, lower star formation efficiencies or suppression of initial infall on to dark matter (DM) haloes is the dominant driver for the suppression of luminous structure formation (Mo et al. 2005). It is more than likely that a combination of the above-mentioned effects will go a long way to alleviating current tensions between models and observations, since current semi-analytical models (SAMs) incorporate several processes in order to generate a deficiency of stellar mass in DM haloes; many of which operate most effectively at low masses (Benson et al. 2003; De Lucia, Kauffmann & White 2004).

Observationally, Zwaan et al. (2005) used the catalogue of 4315 extragalactic H I 21-cm emission line detections from the H I Parkes All Sky Survey (HIPASS; Barnes et al. 2001) and obtained the most accurate measurement of the H I mass function of galaxies to date. The H I mass function (HIMF) is fitted with a Schechter function with a faint-end slope of $-1.37 \pm 0.03$. The sensitivity of this survey was so high that they were able to extend their analysis well down to H I masses of $10^{7.2}\,M_{\odot}$, hence this is the most complete analysis so far. Using these statistical constraints, it has now become possible to make stringent comparisons between theoretical models and observations even in low-mass galaxies.

The physics of cold gas becomes increasingly relevant for constraining galaxy formation models at relatively low masses (dominated by late-type galaxies), where the presence of gas becomes substantial and therefore may break the degeneracies between feedback, star formation and infall processes. Moreover, within the $\Lambda$CDM scenario the H I and $H_2$ mass budgets in galaxies are determined by an intricate offset between several competing processes, all of which have strong mass dependencies. Thus, the present H I and $H_2$ fractions are strong functions of host DM halo mass and the evolutionary history of each individual galaxy. More specifically, the fraction of gas which may be captured by the host DM halo, and in turn removed by feedback, is expected to depend strongly on the binding energy of the gas itself, which is principally determined by the DM halo virial mass and density distribution. Thus, under this framework the observational properties of galaxy populations are strongly influenced by their collective host DM haloes (White & Rees 1978, see Somerville et al. 2008 for a review).

Motivated by the above-mentioned observational advances and theoretical challenges, the primary aim of this work is to investigate the physical origins of the relationships between H I, stellar, and virial masses of galaxies. In order to do this, we compare empirical galaxy relations derived from observational studies, with a physically motivated galaxy formation model. From observational studies (detailed in Evoli, Salucci & Cook 2009), we use a numerical approach (described in Shankar et al. 2006) that relies on the assumption of the existence of a one-to-one mapping between galaxy properties and host DM halo mass. We interpret these results using a physically motivated SAM (see Cook, Lapi & Granato 2009a, hereafter C09, and references therein), which has been shown to reproduce many features of the local galaxy population.

SAMs provide a powerful theoretical framework within which we can explore the range of physical processes (e.g. accretion mechanisms, star formation, SN feedback, black hole growth and feedback etc.) that drive the formation and evolution of galaxies and determine their observable properties (see Somerville et al. 2008; Baugh 2006 for extensive reviews) whilst remaining computationally feasible, allowing for statistical samples of galaxies to be generated.

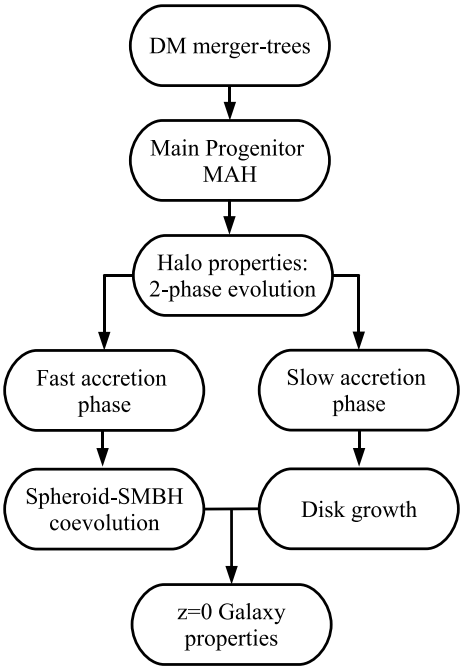


**Figure 1.** Schematic of the model framework, showing how we partition the evolutionary history into spheroid and disc growth epochs, which follow significantly different evolutionary paths for baryonic structure growth and result in the bulge-disc dichotomy observed at $z = 0$.

As is shown in Fig. 1, the backbone to our galaxy formation model is a cosmologically consistent DM halo merger tree, outlining the merging and accretion histories of DM haloes. For the evolution of baryonic structures within these merging trees, we utilize the model of C09, with several modifications. This requires us to partition each mass accretion history (MAH) into two phases: a *'fast accretion'*, merger dominated phase corresponding to spheroid-supermassive black hole (SMBH) co-evolution, followed by a *'slow accretion'*, quiescent phase allowing for disc structure to form around the pre-processed haloes (see also Zhao et al. 2003, hereafter Z03; Mo & Mao 2004), the resulting galaxy properties at $z = 0$ are thus a result of the subgrid baryonic recipes, and the mass accretion histories of their host DM haloes. Within this work, we also expand the previous model by including several additional effects which are thought to be of crucial importance the low-mass gas-rich systems, namely, we model the effects of an ionizing ultraviolet (UV) background, cold accretion flows and exploit a two-phase ISM, where star formation is governed by the surface density of $H_2$.

In summary, we utilize the most up-to-date observations of the stellar and H I mass functions in order to derive relationships between the host DM halo and the galaxy stellar and gas properties, we interpret these results using a physically grounded SAM, and analyse the nature of the results by generating three model realizations, incorporating several contemporary recipes and highlighting how each helps alleviate previous model tensions. The outline of the paper is as follows. In Section 2, we present our SAM, outlining the basic framework from C09, and including the modifications and improvements. In Section 3, we use current observational results of

**Table 1.** Values of the free parameters of our model. We note that the value of $k_{\rm acc}$, despite being a free parameter, has a minor impact on our results.

| Description | Symbol | Fiducial value | Reference in the text | Impact on this work |
|---|---|---|---|---|
| SN feedback efficiency (bulge) | $\epsilon_{\rm SN,b}$ | 0.5 | Equation (15) | Strong |
| SN feedback efficiency (disc) | $\epsilon_{\rm SN,d}$ | 0.7 | Equation (35) | Strong |
| Reservoir growth rate | $A_{\rm res}$ | $10^{-3}\,{\rm M}_{\odot}\,{\rm yr}^{-1}$ | Equation (18) | Strong |
| QSO feedback efficiency | $f_{\rm h}$ | $10^{-4}$ | Equations (22) and (23) | Strong |
| Viscous accretion rate | $k_{\rm acc}$ | $10^{-2}$ | Equation (20) | Weak |

*Note.* – A Romano IMF $\phi(m_\star)$ is adopted: $\phi(m_\star) \propto m_\star^{-1.25}$ for $m_\star \geq {\rm M}_{\odot}$ and $\phi(m_\star) \propto m_\star^{-0.4}$ for $m_\star \leq {\rm M}_{\odot}$.

the stellar and H I mass functions which yield relationships between host DM halo mass and the galaxy stellar and H I components. In Section 4, we present the results of both the observational determinations and the theoretical model comparisons. We conclude in Section 5 by summarizing the main outcomes of this work, discussing the implications and the limitations.

Throughout the paper, we adopt the standard ΛCDM concordance cosmology, as constrained by *Wilkinson Microwave Anisotropy Probe (WMAP)* 5-yr data (Spergel et al. 2007). Specifically, we adopt a flat cosmology with density parameters $\Omega_{\rm M} = 0.27$ and $\Omega_\Lambda = 0.73$, and a Hubble constant $H_0 = 70\,{\rm km\,s^{-1}\,Mpc^{-1}}$.

## 2 PHYSICAL MODEL

We follow the galaxy evolution using a semi-analytical approach, deriving analytical estimates wherever possible to aid simplicity. We track the evolution of DM, hot gas, cold gas and stellar mass using several parametrizations, based on the model described in C09 but with several important modifications.

Namely, we now trace the sequential infall of material on to both spheroid and disc structures and we include the effects of an ionizing UV background, adiabatic contraction of the DM halo and a two-phase ISM. Here, we outline the basic framework for this model (see Table 1).

We initially describe the DM halo evolution using an extended Press–Schechter (EPS) algorithm based on that developed by Parkinson, Cole & Helly (2008). These merger trees have been tuned in order to reproduce the statistics of halo merger and accretion activity obtained from *N*-body simulations of structure formation (Springel et al. 2005). Within our model, we utilize these merger trees by extracting the MAH, i.e. the evolutionary path of a typical DM halo, obtained by tracking the most massive progenitor at each fragmentation event whilst moving from $z = 0$ to progressively higher redshifts (see van den Bosch 2002; C09).

Specifying the DM halo properties, we define the virial radius $r_{\rm vir}$ as that of a spherical volume enclosing an overdensity in a standard way (Bryan & Norman 1998). We compute the density profile for the DM halo using the fitting function of Navarro, Frenk & White (1997, hereafter NFW),

$$\rho_{\rm NFW}(r) = \rho_{\rm s} \left(\frac{r}{r_{\rm s}}\right)^{-1} \left(1 + \frac{r}{r_{\rm s}}\right)^{-2} . \quad (1)$$

In order to define the scale radius $r_{\rm s}$ for our NFW profile, we introduce the *concentration parameter*, which is defined to be $c(z) \equiv r_{\rm vir}/r_{\rm s}$. This quantity has been studied by several authors (see Bullock et al. 2001; Z03; Macciò et al. 2007) who found large scatter for a fixed halo mass, but to scale generally with the MAH of the halo. We adopt here the $z$ evolution of Z03,

$$[\ln(1+c) - c/(1+c)]c^{-3\alpha} \propto H(z)^{2\alpha} M_{\rm vir}(z)^{1-\alpha} , \quad (2)$$

where $\alpha$ is a piecewise function which can be found in Z03 and where the normalization can be fixed using the expression given by Macciò et al. (2007) at $z = 0$,

$$\log c_0 = 1.071 - 0.098 \left[\log\left(\frac{M_{\rm vir,0}}{{\rm M}_{\odot}}\right) - 12\right] . \quad (3)$$

From this, the scale density may be computed for a general profile to be $\rho_{\rm s} = M_{\rm vir}(z)/[4\pi\, r_{\rm s}^3\, f(c)]$, with

$$f(c) = \ln(1+c) - \frac{c}{1+c} . \quad (4)$$

Finally, we specify the angular momentum properties of each halo through the *spin parameter*, defined to be $\lambda = J_{\rm vir} E_{\rm vir}^{1/2} M_{\rm vir}^{5/2} G^{-1}$, where $E_{\rm vir}$ and $J_{\rm vir}$ are the total energy and angular momentum of the halo. Assuming that a DM halo acquires its angular momentum through tidal torques with the surrounding medium, λ remains constant. It has been shown (Cole & Lacey 1996) that the spin parameter varies little with cosmic epoch, halo mass or environment and for a sample of haloes is well fitted by a log-normal distribution (where $\bar{\lambda} = 0.04$ and $\sigma = 0.5$). However, for simplicity, here we assume that each halo has a parameter value of $\lambda = 0.04$ which remains constant throughout the DM halo evolution.

Several studies have shown the concentration evolution to be strongly correlated to the MAH of the halo (Z03; Li et al. 2007; Lu et al. 2006), finding that DM haloes generally acquire their mass in two distinct phases; an initial phase characterized by rapid halo growth through major merger events, where the halo core structure forms, causing the gravitational potential to fluctuate rapidly, followed by a slower, more quiescent growth predominantly through accretion of material on to the outer regions of the halo. These two different modes are reflected in the evolution of the concentration parameter, which remains roughly constant during the 'fast accretion' phase and steadily increases during the 'slow accretion' phase. The transition redshift $z_{\rm t}$ between these two phases can therefore be calculated using the expression for the concentration parameter evolution given in Z03,

$$\frac{[\ln(1+c_{\rm t}) - c_{\rm t}/(1+c_{\rm t})]c^{-3\alpha}}{[\ln(1+c_0) - c_0/(1+c_0)]c_0^{-3\alpha}} = \left[\frac{H(z_{\rm t})}{H_0}\right]^{2\alpha} \left[\frac{M_{\rm vir}(z_{\rm t})}{M_{\rm vir,0}}\right]^{1-\alpha} , \quad (5)$$

where $H(z)$ is the Hubble radius, '0' denotes quantities evaluated at the present cosmic time, and $c_{\rm t} = 4$ and $\alpha = 0.48$ are scaled to match *N*-body simulations as in Z03.

By associating the two phases of DM evolution to two growth mechanisms for the baryonic sector, the fast and slow phases give rise to the formation of bulges and discs, respectively (Mo & Mao 2004; C09). Since within the 'fast accretion' phase, angular momentum may be readily lost by rapidly merging clumps of material, in an implicit merger scenario, resulting in the formation of a spheroidal structure, followed by the quiescent dissipationless infall of material in order to form discs (see C09 for a more detailed analysis and

justifications of this). At difference with the prescriptions outlined in C09, here we expand our model to include the symbiotic infall of baryonic material as the DM halo evolves, thus

$$\dot{M}_{\rm inf} = f_{\rm coll}\dot{M}_{\rm vir}\,. \tag{6}$$

We include the effects of an ionizing radiation background taking the prescriptions outlined in (Gnedin et al. 2004; Somerville et al. 2008), which is able to partially reduce the baryonic content in low-mass systems, thus

$$f_{\rm coll}(M_{\rm vir}, z) = \frac{\Omega_{\rm b}/\,\Omega_{\rm m}}{(1+0.26M_{\rm f}(z)/M_{\rm vir})^3}\,, \tag{7}$$

where $M_{\rm f}(z)$ is the filtering mass at a given redshift, computed using the equations in (Kravtsov, Gnedin & Kyplin 2004, appendix B). A second improvement over our previous model (C09) is to include the effects of cold accretion flows, shown to be the predominant mechanism leading to the formation of low-mass systems. Below a critical mass,

$$M_{\rm c} = M_{\rm s}\max[1, 10^{1.3(z-z_{\rm c})}]\,, \tag{8}$$

where $M_{\rm s} = 2\times10^{12}\,{\rm M}_\odot$ and $z_{\rm c} = 3.2$, we assume that all gas accreted on to DM haloes is not shock heated to the virial temperature of the DM halo, but streams in on a dynamical time (see Cattaneo et al. 2006; Dekel et al. 2009). We note that below the shock heating mass scale it has been shown that rapid cooling does not allow for the formation of a stable virial shock (Keres et al. 2005) resulting in gas flowing unperturbed into the central regions of the DM halo. Thus, in haloes below this mass the collapse happens on the dynamical time-scale of the system ($t_{\rm coll} = t_{\rm dyn}$), whereas in haloes above this mass $t_{\rm coll} = \max[t_{\rm dyn}, t_{\rm cool}]$, where the cooling time-scale $t_{\rm cool}$ is computed in a standard way, assuming material is shock heated to the virial temperature. The effects of this cold accretion are to moderately enhance star formation at high redshifts relative to the scenario where all material is shock heated, in this way, we model the infall and cooling dynamics using the most current recipes (see Somerville et al. 2008).

In order to calculate the cooling time of the hot gas phase, we assume an isothermal gas in hydrostatic equilibrium within the NFW profile, such that

$$\rho_{\rm hot}(r) = \rho_0\exp\left[\frac{-27}{2}\beta\left\{1-\frac{\ln(1+r/r_{\rm s})}{r/r_{\rm s}}\right\}\right], \tag{9}$$

with

$$\beta = \frac{8\pi\mu m_p G\rho_{\rm s}r_{\rm s}^2}{27k_BT_{\rm vir}}\,, \tag{10}$$

where $T_{\rm vir}$ is the virial temperature, $\mu$ is the mean molecular mass and $\rho_0$ is calculated by normalizing to the total hot gas mass at any given redshift. Also, we assume that the cooling function $\Lambda(T, Z)$ is given by the tabulated function of Sutherland & Dopita (1993), and assume that the infalling baryonic material is near unprocessed and therefore has primordial metallicity, $Z = 10^{-3}\,{\rm Z}_\odot$.

### 2.1 Dissipative gas collapse

During the high-redshift domain, it has been shown that the majority of the angular momentum of the collapsing proto-galactic gas dissipates as it collapses and condenses to the centres of DM haloes (see Navarro & Steinmetz 2000). Also, within C09, we show that during the early collapse phase, DM halo subunits merge on time-scales shorter than the overall dynamical time of the forming halo. Therefore, within the 'fast accretion' phase, we neglect the effects of angular momentum of cooling proto-galactic gas, which will result in the formation of a spheroidal gaseous system at a rate

$$\dot{M}_{\rm coll}(z) = 4\pi\int_0^{r_{\rm vir}(z)}\frac{r^2\rho_{\rm hot}(r,z)}{t_{\rm coll}(r,z)}{\rm d}r\,, \tag{11}$$

where $t_{\rm coll}(r,\ z)$ is determined by the cold-accretion recipe of equations (8)–(10). We denote this cold gas spheroidal component ('gaseous bulge'), which acts as a reservoir for star formation, by $M_{\rm b,gas}(t)$, and stress that besides dissipative collapse, it can also grow through merger events and disc instabilities. Also, our model includes other two components: a spheroidal stellar component ('stellar bulge') $M_{\rm b,star}(t)$, and a low angular momentum cold gas reservoir $M_{\rm res}(t)$, which acts as a source of material eligible to accrete on to a central black hole.

For simplicity,[1] we assume that the reservoir can be described by an exponential disc surface density,

$$\Sigma_{\rm res}(r,z) = \Sigma_0(z){\rm e}^{-r/r_{\rm res}(z)}\,, \tag{12}$$

with the scale radius $r_{\rm res}$ being proportional to the influence radius of the SMBH ($r_{\rm res} = \alpha GM_{\rm SMBH}/V_{\rm vir}^2$, with $\alpha\approx100$). Also, since we have no a priori information about the geometric distribution of baryonic matter within the bulge system, and since the dynamics and thus evolution of disc structure are correlated to the mass and geometry of the bulge structure, we assume that the bulge stellar and gaseous masses settle into a Hernquist density profile,

$$\rho_{\rm b}^*(r) = \frac{M_{\rm b}^*}{2\pi}\frac{r_{\rm b}}{r(r+r_{\rm b})^3}\,,\quad *={\rm stars,\,gas}\,, \tag{13}$$

where the scale radius of this profile is related to the half light radius by $r_{\rm b} = 1.8152R_{\rm eff}$. Using the fitting of Shen et al. (2003), we take the parametrization as a function of bulge mass to be

$$\log(R_{\rm eff}) = \left\{\begin{array}{ll}-5.54+0.56\log(M_{\rm b}) & [\log(M_{\rm b})>10.3]\\ -1.21+0.14\log(M_{\rm b}) & [\log(M_{\rm b})\le10.3].\end{array}\right\}.$$

The star formation rate (SFR) per annulus in the gaseous bulge may be computed as

$$\frac{{\rm d}\psi_{\rm b}}{{\rm d}r}(r,t) = 4\pi r^2\frac{\rho_{b,{\rm gas}}(r)}{t_{gas}(r)}\,, \tag{14}$$

where $t_{\rm gas}(r)$ is the dynamical time for the gas in the bulge. Therefore, in order to compute the total SFR, we must integrate this expression over all radii.

Energetic feedback due to supernova events may transfer significant energy into the cold ISM, causing it to be reheated and ejected from the system. Therefore, by considering energy balance in the ISM, supernovae feedback is able to remove gas from the bulge at a rate,

$$\dot{M}_{b,{\rm gas}}^{SN}(t) = -\int\frac{\epsilon_{\rm SN,b}E_{\rm SN}\eta_{\rm SN}{\rm d}\psi_{\rm b}(r,t)/{\rm d}r}{\phi(r,t)}{\rm d}r\,, \tag{15}$$

where $\eta_{\rm SN}$ is the number of Type II supernovae expected per solar mass of stars formed[2], $E_{\rm SN}$ is the kinetic energy released per supernova event, and $\epsilon_{\rm SN,b}$ is the efficiency of supernovae energy transfer

[1] We need to make an assumption about the reservoir geometry because that is needed to calculate the velocity of the composite system $V_{\rm c}$ (needed e.g. in equations 27 and 32, the adiabatic halo contraction factor $\Gamma$, equations 28 and 29), and the gravitational potential $\phi$ of the composite system appearing in equations (15) and (34). However, the geometry of the reservoir is not expected to have a major impact on our results, given its small size relative to the other components.

[2] A Romano initial mass function (IMF) $\phi(m_\star)$ is adopted: $\phi(m_\star)\propto m_\star^{-1.25}$ for $m_\star\ge{\rm M}_\odot$, and $\phi(m_\star)\propto m_\star^{-0.4}$ for $m_\star\le{\rm M}_\odot$. This gives $\eta_{\rm SN} = 5\times10^{-3}\,{\rm M}_\odot^{-1}$.

used to remove the cold gas. Finally, $\phi(r,\, t)$ is the gravitational potential of the composite system (bulge, reservoir, disc and DM). Therefore, using this prescription, we see that supernovae feedback is particularly efficient in smaller haloes with shallower gravitational potential wells, but relatively inefficient in larger haloes. Using scaling relations, Granato et al. (2000) were able to show that stars form faster in larger systems, thus exhibiting the observed 'anti-hierarchical' behaviour of spheroid galaxies.

A growing body of evidence is now showing that the evolution of both the SFR within spheroids and the fuelling of SMBH's are proportional to one another (Haiman, Ciotti & Ostriker 2004). A proposed mechanism to account for this phenomenon has been discussed (Kawakatu, Umemura & Mori 2003): radiation drag due to stellar radiation may result in the loss of angular momentum at a rate well approximated within a clumpy ISM by

$$\frac{\mathrm{d}\ln(J)}{\mathrm{d}t} \approx \frac{L_{\rm sph}}{c^2 M_{b,\rm gas}}(1-e^{-\tau})\,, \tag{16}$$

where $L_{\rm sph}$ is the total stellar luminosity and $\tau$ is the effective optical depth of the spheroid ($\tau = \bar{\tau} N_{\rm int}$, where $\bar{\tau}$ is the average optical depth, and $N_{\rm int}$ is the average number of clouds intersecting a light path). Upon loss of angular momentum, this gas may flow into the nuclear region, generating the reservoir of low-J material which fuels BH growth at the rate (Granato et al. 2004)

$$\dot{M}_{\rm res} \approx 1.2\times10^{-3}\psi_{\rm b}(t)(1-e^{-\tau})\,{\rm M}_\odot\,{\rm yr}^{-1}\,. \tag{17}$$

We note that, within this work we assume that $\tau$ is constant for simplicity, which allows one to rewrite equation (17) as

$$\dot{M}_{\rm res} = A_{\rm res}\psi_{\rm b}(t)\,, \tag{18}$$

where $A_{\rm res}$ is a free parameter. The cold gas stored in the reservoir is then expected to accrete on to the central SMBH with an accretion rate

$$\dot{M}_{\rm bh} = \min[\dot{M}_{\rm visc},\, \dot{M}_{\rm edd}]. \tag{19}$$

In this formula, the viscous accretion rate is given by (Granato et al. 2004)

$$\dot{M}_{\rm visc} = k_{\rm acc}\frac{\sigma^3}{G}\left(\frac{M_{\rm res}}{M_{bh}}\right)\,, \tag{20}$$

where $k_{\rm acc} \approx 10^{-2}$, whilst the Eddington accretion rate is simply $\dot{M}_{\rm edd} = L_{\rm edd}/\eta c^2$, with[3] $\eta \approx 0.15$ and

$$L_{\rm Edd} \approx 1.26\times10^{46}\frac{M_{\rm BH}(t)}{10^8\,{\rm M}_\odot}{\rm erg\ s}^{-1}. \tag{21}$$

Quasi-stellar object (QSO) activity affects the ISM of the host galaxy and also the surrounding intergalactic medium through both radiative heating and the kinetic energy input through gas outflows. Assuming that a fraction $f_{\rm h}$ (which we treat as a free parameter) of the SMBH luminosity $L_{\rm h}$ is transferred into the cold and hot gas phases, it is possible to compute the amount of cold and hot gas which is removed from the hot gas and gaseous bulge phases as in Granato et al. (2004),

$$\dot{M}^{\rm QSO}_{b,\rm gas} = f_{\rm h}\frac{2}{3}\frac{L_{\rm h}}{\sigma^2}\frac{M_{b,\rm gas}}{M_{\rm hot}+M_{b,\rm gas}}\,, \tag{22}$$

$$\dot{M}^{\rm QSO}_{\rm hot} = f_{\rm h}\frac{2}{3}\frac{L_{\rm h}}{\sigma^2}\frac{M_{\rm hot}}{M_{\rm hot}+M_{b,\rm gas}}\,, \tag{23}$$

[3] This value of $\eta$ corresponds to rapidly spinning SMBH with spin parameter $a \approx 0.9$ (Bardeen 1970).

where $\sigma = 0.65V_{\rm vir}$. This material is assumed to be ejected from the system.

For the chemical evolution of the cold bulge gas, we use the simple instant-recycling approximation (IRA), whereby a fraction of mass is instantly returned into the cold gas phase in the form of processed material.[4] In particular, this implies that the effective SFR which enters the evolution equations for the gas and star bulge masses is given by

$$\dot{M}^{\rm SFR}_{\rm b}(t) = (1-R)\int\frac{\psi_{\rm b}}{\mathrm{d}r}(r,t)\mathrm{d}r\,, \tag{24}$$

with $R = 0.25$. Also, we assume that $M_{\rm hydrogen} = 0.71M_{\rm cold}$, where the factor takes into account the contribution of Helium and other heavier elements.

### 2.2 Dissipationless gas collapse

By assuming that material may collapse to form a cool gaseous disc structure during the slow accretion phase, we may add material to the disc structure at a rate which is given, as in the spheroidal case, by

$$\dot{M}_{\rm coll}(z) = 4\pi\int_0^{r_{\rm vir}(z)}\frac{r^2\rho_{\rm hot}(r,z)}{t_{\rm coll}(r,z)}\mathrm{d}r\,, \tag{25}$$

where $t_{\rm coll}(r, z)$ is determined again by the cold-accretion determinations (see equations 8–10). If we assume a dissipationless collapse of material upon cooling within the DM halo, we may relate the dark halo virial radius and spin parameter to the forming disc scale radius. In particular, if we assume an exponential disc surface density profile for the stellar and gaseous components,

$$\Sigma^*_{\rm d}(r,z) = \Sigma^*_0(z){\rm e}^{-r/r_{\rm d}(z)}\,,\quad *={\rm stars,\,gas}\,, \tag{26}$$

the disc scale radius $r_{\rm d}(z)$ evolves according to the scaling $r_{\rm d}(z) = (2\pi)^{-1/2}(j_{\rm d}/m_{\rm d})\lambda r_{\rm vir}(z)f(c)^{-1/2}f_r(\lambda,\, c,\, m_{\rm d}j_{\rm d})$. The function $f(\lambda,\, c,\, m_{\rm d}\ j_{\rm d})$ may be exactly determined through (Mo, Mao & White 1998)

$$f(\lambda,c,m_{\rm d},\,j_{\rm d}) = 2\left[\int_0^\infty e^{-u}u^2\frac{V_{\rm c}(r_{\rm d}u)}{V_{\rm c}(r_{\rm vir})}\mathrm{d}u\right]^{-1}\,, \tag{27}$$

where $V_{\rm c}(r)$ is the velocity profile of the composite system (bulge, reservoir, disc and DM) and where $m_{\rm d}$ and $j_{\rm d}$ are the ratios between the total mass and angular momentum of the disc component and the DM halo mass. More specifically, we take $m_{\rm d} = (M^{\rm stars}_{\rm d} + M^{\rm gas}_{\rm d})/M_{\rm vir}$, and we assume $j_{\rm d} = m_{\rm d}$ (Mo et al. 1998).

In order to account for adiabatic halo response, we take the standard prescription of Blumenthal et al. (1986). In particular, denoting by $M_X(r)$ the mass of a given component '$X$' enclosed by a radius $r$, from the angular momentum conservation one obtains

$$M_{\rm i}(r_{\rm i})r_{\rm i} = M_{\rm f}(r_{\rm f})r_{\rm f}\,, \tag{28}$$

where $r_{\rm i}$ and $r_{\rm f}$ are respectively the initial and final radius of the shell under consideration, the initial mass distribution $M_{\rm i}(r_{\rm i})$ is simply given by the NFW density profile, while $M_{\rm f}(r_{\rm f})$ is the final mass distribution. Also, mass conservation easily gives

$$\begin{aligned} M_{\rm f}(r_{\rm f}) &= M_{\rm d}(r_{\rm f}) + M_{\rm b}(r_{\rm f}) + M_{\rm DM}(r_{\rm f}) + M_{\rm res}(r_{\rm f}) \\ &= M_{\rm d}(r_{\rm f}) + M_{\rm b}(r_{\rm f}) + M_{\rm res}(r_{\rm f}) + (1-f_{\rm gal})M_{\rm i}(r_{\rm i})\,, \end{aligned} \tag{29}$$

[4] We adopt a Romano et al. (2005) IMF, which has the standard Salpeter slope 1.25 in the high mass tail, and flattens to a slope 0.4 below 1 $\mathrm{M}_\odot$. As shown in Romano et al. (2005), this performs better than the Salpeter one in reproducing the detailed chemical properties of elliptical galaxies.

where $f_{\rm gal} = M_{\rm gal}/M_{\rm vir}$ (with $M_{\rm gal} = M_{\rm d} + M_{\rm b} + M_{\rm res}$). By assuming spherical collapse without shell crossing, one can adopt the ansatz $r_{\rm f} = \Gamma r_{\rm i}$, with $\Gamma$ = const (Blumenthal 1986), and equations (28) and (29) may be solved numerically for the contraction factor $\Gamma$.

When the surface density of the gaseous disc increases, the cold gas becomes available to form stars. However, at present, star formation is poorly understood from both a microscopic, and large scales. Therefore, we parametrize the star formation using an empirical *Schmidt law* (Kennicutt 1998) whereby the SFR is related to the surface density of cold disc gas,

$$\dot{\Sigma}_{\rm sfr}(r,z) = \epsilon_{\rm sf}\left[\frac{\Sigma_{\rm d}^{\rm gas}(r,z)}{{\rm M}_\odot\,{\rm pc}^{-2}}\right]^n {\rm M}_\odot\,{\rm kpc}^{-2}\,{\rm yr}^{-1}, \quad (30)$$

where $\epsilon_{\rm sf} = 2.5 \times 10^{-4}$ controls the star formation efficiency and $n = 1.4$ is fixed to match the properties of spiral galaxies. This law is empirically proven to hold over many orders of magnitude of gas surface density, but was shown to break down at large radii (Kennicutt 1998) where the surface density drops below a critical value, roughly corresponding to the Toomre (1964) stability criterion. We take this critical surface density to be

$$\Sigma_{\rm c}(r) = \frac{\sigma_{\rm g}\kappa(r)}{3.36GQ}, \quad (31)$$

Toomre (1964). Where $\sigma_{\rm g} = 6\,{\rm km\,s}^{-1}$ is the velocity dispersion of the gas, $Q = 1.5$ is a dimensionless constant, and $\kappa(r)$ is the epicyclic frequency, given by

$$\kappa(r) = \sqrt{2}\frac{V_{\rm c}(r)}{r}\left[1 + \frac{r}{V_{\rm c}(r)}\frac{{\rm d}V_{\rm c}(r)}{{\rm d}r}\right]^{1/2}. \quad (32)$$

Therefore, the conversion rate of gas mass to stellar mass is computed as

$$\psi_{\rm d}(z) = 2\pi\epsilon_{\rm sf}\int_0^{r_{\rm c}} r\,\Sigma_{\rm d,\,gas}^n(r,z){\rm d}r, \quad (33)$$

where $r_{\rm c}$ may be calculated by solving $\Sigma_{\rm d}^{\rm gas}(r_{\rm c},z) = \Sigma_{\rm c}(r_{\rm c})$ for $r_{\rm c}$.

In order to account for feedback due to supernovae events, we may compute the amount of cold gas which is ejected from the system at each disc radius. In order to remove this cold gas from the disc, the supernovae feedback must be sufficient to unbind it, therefore we compare the amount of energy released through supernovae events at each disc radius with the binding energy at the same radius,

$$\dot{\Sigma}_{\rm SN}(r,z) = -\frac{\epsilon_{\rm SN,d}E_{\rm SN}\eta_{\rm SN}\dot{\Sigma}_{\rm sfr}(r,z)}{\phi(r,z)}, \quad (34)$$

where $\phi(r,z)$ again is the binding energy of the composite system (bulge, disc, reservoir and DM). The total amount of cold gas ejected from the system is then given by

$$\dot{M}_{\rm SN}^{\rm d}(z) = 2\pi\int_0^{r_{\rm vir}} r\dot{\Sigma}_{\rm SN}(r,z){\rm d}r. \quad (35)$$

For the chemical evolution of the cold disc gas, we use again the IRA approximation, and the 'effective' SFR which enter the evolution equations for the gas and star disc masses is given by

$$\dot{M}_{\rm SFR}^{\rm d}(z) = (1-R)\psi_{\rm d}(z), \quad (36)$$

with $R = 0.25$. Also, we assume again that $M_{\rm hydrogen} = 0.71M_{\rm cold}$.

Finally, it is known that when discs become self-gravitating they are likely to develop bar instabilities, get disrupted and transfer material to the spheroidal component (Christodoulou, Shlosman & Tohline 1995). We therefore assume that a stellar or gaseous disc is stable if

$$\frac{V_{\rm c}(2.2r_{\rm d})}{(GM_{\rm disc}^*/r_{\rm d})^{1/2}} > \alpha_{\rm crit}^* \quad * = {\rm stars}\,,\,{\rm gas}\,, \quad (37)$$

where $\alpha_{\rm crit}^{\rm stars} = 1.1$ and $\alpha_{\rm crit}^{\rm gas} = 0.9$ (see Mo et al. 1998 and references therein). If we find that discs become unstable, we assume they get disrupted in a dynamical time and transfer their material (either stars or gas) to the bulge components.

### 2.3 Improved star formation law

Assuming that star formation may only take place inside dense molecular clouds several authors have shown that the Schmidt–Kennicutt star formation law (equation 30) may be reproduced within large mass systems by assuming that the SFR is proportional to the molecular cloud mass (Blitz & Rosolowsky 2006; Dutton & van den Bosch 2009), thus

$$\dot{\Sigma}_{\rm sfr} = \tilde{\epsilon}_{\rm sf}\Sigma_{\rm mol,HCN}, \quad (38)$$

Where $\tilde{\epsilon}_{\rm sf} = 13\,{\rm Gyr}^{-1}$ and $\Sigma_{\rm mol,HCN} = f_{\rm mol}R_{\rm HCN}$ is the molecular mass surface density as traced by HCN (see Gao & Solomon 2004; Wu et al. 2005). Thus, calculating the ratio of molecular gas to atomic gas allows us to compute the SFR at all scales. The fraction of gas in discs which is molecular has been extensively analysed, and shown to be closely related to the mid-plane pressure within discs (Blitz & Rosolowsky 2006), given by

$$P_{\rm mp} = \frac{\pi}{2}G\Sigma_{\rm g}[\Sigma_{\rm g} + (\sigma_{\rm g}/\sigma_{\rm s})\Sigma_{\rm s}], \quad (39)$$

where, following the detailed prescriptions of Dutton & van den Bosch (2009), assuming a constant $\sigma_{\rm g}/\sigma_{\rm s} = 0.1$. Relating the mid-plane pressure to the formation of molecular clouds yields

$$R_{\rm mol} = \frac{\Sigma_{\rm mol}}{\Sigma_{\rm atom}} = \left(\frac{P_{\rm mp}/k}{4.3\times10^4}\right)^{0.92}. \quad (40)$$

Thus, the molecular fraction is given by $f_{\rm mol} = R_{\rm mol}/(R_{\rm mol}+1)$, in order to relate this to the HCN fraction, we must further compute the fitting relation of Blitz & Rosolowsky (2006),

$$R_{\rm HCN} = 0.1 * \left[1 + \Sigma_{\rm mol}/(200\,{\rm M}_\odot\,{\rm pc}^{-2})\right]^{0.4}. \quad (41)$$

Therefore, we find that, in the high-mass (and thus density) galaxies, where the molecular fraction is typically $\approx$1, we recover the standard Schmidt–Kennicutt star formation power law, with exponent 1.4, whereas in the low-density galaxies we asymptote towards an exponent of 2.84, suppressing star formation in these systems, in accordance with observations (see Dutton & van den Bosch 2009; Blitz & Rosolowsky 2006 for a detailed description). Thus, throughout the evolution of each galaxy, we partition the ISM into H I and $H_2$ components using the above relations, and compute the star formation law (and therefore supernovae feedback) using equation (42) in order to self-consistently model each galaxy under this improved star formation law.

## 3 THE H I MASS RELATIONSHIPS

In order to investigate the relationship between the stellar and the gas component in late-type galaxies, we follow the procedure already exploited by Shankar et al. (2006), and discussed in detail in Evoli et al. (2009). We defer the reader to these papers for a more detailed discussion and highlight the main results here. If two galaxy properties, $q$ and $p$, obey a one-to-one relationship, we can write

$$\phi(p)\frac{{\rm d}p}{{\rm d}q}{\rm d}q = \psi(q){\rm d}q, \quad (42)$$

where $\psi(q)$ is the number density of galaxies with measured property between $q$ and $q + {\rm d}q$ and $\phi(p)$ is the corresponding number

density for the variable $p$. The solution is based on a numerical scheme that imposes that the number of galaxies with $q$ above a certain value $\bar{q}$ must be equal to the number of galaxies with $p$ above $\bar{p}$, i.e.

$$\int_{\bar{p}}^{\infty} \phi(p)\mathrm{d}p = \int_{\bar{q}}^{\infty} \psi(q)\mathrm{d}q. \quad (43)$$

In the following, the HIMF is given by $p = M_{\rm H\,I}$ and $\phi(p) =$ HIMF ($M_{\rm H\,I}$), while the variable $q$ is the stellar mass ($M_*$) and $\psi(q)$ the corresponding galactic stellar mass function (GSMF ($M_*$)).

Using the H I Parkes All-Sky Survey HIPASS (Meyer et al. 2004), it has become possible to map the distribution of H I in the nearby Universe. The HIMF has been fitted with a Schecter function with a power index of $\alpha = -1.37 \pm 0.03$, a characteristic mass of $\log(M^*_{H\,I}/\,\mathrm{M}_\odot) = 9.80 \pm 0.03\,h_{75}^{-2}$ and a normalization of $\theta^* = (6.0 \pm 0.8) \times 10^{-3}\,h_{75}^3\,\mathrm{Mpc}^{-3}\,\mathrm{dex}^{-1}$. Nakamura et al. (2003) estimated the luminosity function in the $r^*$ band for early- and late-type galaxies separately. Shankar et al. (2006) used the results of Zucca et al. (1997) and Loveday (1998) to extend these results to lower luminosities and giving a good fit for the late-type galaxy luminosity function in the range $10^7\,\mathrm{L}_\odot < L_r < 3 \times 10^{11}\,\mathrm{L}_\odot$. The GSMF, holding over the mass range $10^8 < M_* < 10^{12}$ is compared with the one of Bell et al. (2003a), and is in good agreement within the uncertainties due to the mass-to-light ratio, estimated to be around 30 per cent.

The correlation of galaxy properties with the halo mass ($M_{\rm h}$) is extremely relevant in the framework of galaxy formation theories. To constrain such a relation, we used the association between the stellar mass and the host halo mass derived in Shankar et al. 2006 (equation 12 and Fig. 1 therein), which has been obtained with the method already mentioned, but using either for the stellar mass function and the galactic halo mass function a fitting of the observations/simulation for all the galaxies. Finding relations between each of the mass components within galaxies is of great importance because it allows for constraints on the direct outputs from models, not requiring significant post processing, and providing useful links between the dark and luminous components of galaxies. We find that the results of the numerical outputs may be well approximated by the following analytic fitting functions:

$$\frac{M_{H\,I}}{2.38 \times 10^8\,\mathrm{M}_\odot} = \frac{(M_*/6.1 \times 10^7\,\mathrm{M}_\odot)^{2.37}}{1 + (M_*/6.1 \times 10^7\,\mathrm{M}_\odot)^{1.81}}, \quad (44)$$

$$\frac{M_{H\,I}}{6.07 \times 10^8\,\mathrm{M}_\odot} = \frac{(M_{\rm vir}/5.7 \times 10^{10}\,\mathrm{M}_\odot)^{5.82}}{1 + (M_{\rm vir}/5.7 \times 10^{10}\,\mathrm{M}_\odot)^{4.76}}. \quad (45)$$

Fig. 2 shows the ratio of the baryonic mass components (stellar, gas and total) to the initial baryon mass associated with each DM halo obtained using the above-mentioned methods (and explained in Evoli et al. 2009), illustrating the inefficiency of galaxies, especially those of low halo mass, in retaining baryons. These relationships can be used to tightly constrain theoretical galaxy formation models in order to interpret the physical processes relevant to shape these relations.

## 4 RESULTS

Throughout this section, we present the results of model realizations, each comprising of a sample of $\approx 10^3$ galaxies in logarithmic virial mass increments in the mass range $9.5 < \log(M_v(z = 0)/\mathrm{M}_\odot) < 13.5$ in order to encompass the observational range of galaxy-hosting DM haloes. In order to make statistical predictions with each generated galaxy sample at $z = 0$, we weight each DM halo with the GHMF, which mirrors the Sheth & Tormen (2002) mass function within most galaxy sized DM haloes, but is derived in order to account for the increasing probability of multiple galaxy occupation in the highest mass haloes (see Shankar et al. 2006). Throughout this section, we also plot the results for 'early' and 'late' type galaxies, by parting the populations into $[M_{\rm bulge}/M_{\rm total}] > 0.5$ and $[M_{\rm bulge}/M_{\rm total}] < 0.5$, respectively.

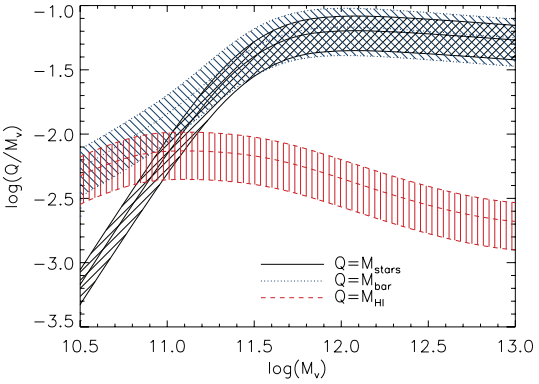


**Figure 2.** The derived relationships between virial mass and; stellar (solid/black), H I (dashed/red) and baryonic (dotted/blue) components. Shaded regions corresponding to the $1\sigma$ Gaussian errors associated with the observational determinations.

### 4.1 Component evolution

In order to illustrate the general behaviour of our galaxy formation framework, Fig. 3 highlights the evolution of each mass component from $z = 8$ up to the present epoch. In the left-hand, centre and right-hand panels, we show a low-, intermediate- and high-mass galaxy, respectively, in order to highlight typical model outputs for each system. As can be seen, the evolution of each galaxy differs significantly due both to scatter at each mass through Monte Carlo selected mass accretion histories, and to the relative differences in efficiencies of the competing processes of infall, star formation and feedback on different mass scales.

We find, in broad agreement with observations, that a typical low-mass galaxy [with $M_v(z = 0) \approx 10^{10}\,\mathrm{M}_\odot$] supports the growth of a disc structure from high redshifts showing extended star formation up to $z = 0$ resulting in a gas-rich disc dominated galaxy with a negligible bulge component. In intermediate mass, $\mathrm{L}_\odot$ galaxies, at high-redshifts gaseous collapse on to a spheroid system results in the co-evolution of SMBH's and the spheroidal component resulting in a gas poor, *'red and dead'* spheroidal stellar component which acts as the bulge within the resultant formed galaxy as the disc component grows steadily from $z \leq 1.5$. The high-mass galaxy shows rapid early growth of the SMBH and spheroid component, followed by an epoch of dormancy in the star formation, no significant disc structure may form in these systems and ongoing star formation is prevented due to the presence of a large SMBH which acts to effectively expel any residual gas which may infall later, only allowing for extremely mild star formation following the main growth phase. The resulting galaxy spheroidal component thus comprises an old stellar population, with little gas and negligible star formation, and the disc component is over an order of magnitude smaller than the bulge, and gas rich, showing little star formation.

These results are consistent with the evolutionary histories tuned to match the chemical properties of local galaxies of different morphological type and different host halo masses (Calura, Pipino &

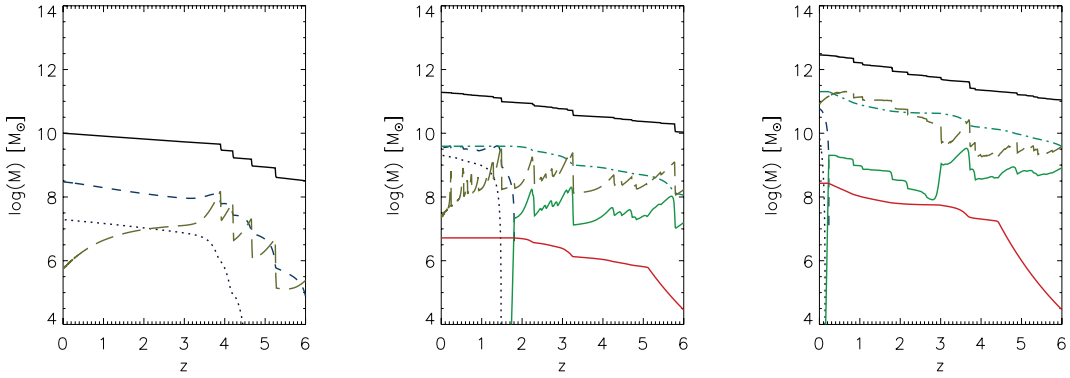


**Figure 3.** The evolution of typical model galaxies; a low-mass disc-dominated galaxy (left-hand panel), an $L_{\odot}$ galaxy with both bulge and discs present (middle panel), and a high mass, spheroid dominated galaxy (right-hand panel): DM mass (solid/black), hot gas (long-dash/brown), disc gas (short-dash/blue), disc stars (dotted/purple), bulge gas (triple-dot–dashed/green), bulge stars (dot–dashed/aquamarine), BH mass (solid/red).

Matteucci 2008 and references therein), which have also been shown to be consistent with photometry within the local Universe (Schurer et al. 2009) and are generally in agreement with observations of statistical samples of galaxies (Driver et al. 2006), however, as can also be seen, due to the stochastic nature of the model, fluctuations in galaxy properties are expected, and thus we must revert to statistically representative samples of galaxy populations in order to make more robust comparisons.

Within these systems in-falling baryonic material is shock heated and therefore may form a static atmosphere of hot gas. Feedback from a growing SMBH may thus halt the cooling of this gas, quenching star formation and sweeping out the ISM (see Granato et al. 2004). Within these systems, it is thought that baryonic material is shock heated and therefore cooling, and feedback from a growing SMBH may quench star formation by sweeping out the ISM (see Granato et al. 2004)

### 4.2 Stellar and Baryon mass functions

The local stellar and baryonic mass functions provide a powerful constraint on theoretical models of galaxy formation: encompassing much of the relevant physical processes which determine the assembly of baryons within DM haloes.

In order for models to reproduce observational results, it has become clear that physical processes of gas accretion, supernovae feedback and photoionization are most effective in the lowest mass DM haloes, where the shallow potential wells are inefficient at trapping and holding baryonic material. Thus, these processes drive the evolution of the faint-end slope of the mass functions (Benson et al. 2002), whereas the brightest galaxies (above $L_*$) are embedded within large DM haloes which effectively trap baryonic material. Within these systems, in-falling baryonic material is shock heated and therefore may form a static atmosphere of hot gas. Feedback from a growing SMBH may thus halt the cooling of this gas, quenching star formation and sweeping out the ISM (see Granato et al. 2004). Coupled with the increasing subhalo contribution (through the cluster mass function) whereby in DM haloes with $M_v(z = 0) > 10^{13}$, the probability of a single galaxy occupation is low, gives rise to the relatively sharp cut-off of stellar mass within the largest DM haloes (see Shankar et al. 2006; Somerville et al. 2008, and contained references).

Rather than computing the spectral energy distribution (SED) assuming any mass-to-light ratio for each model galaxy (relying upon further model assumptions such as the dust-to-gas ratio, molecular cloud structure and optical depth etc.) by comparing the stellar and total baryon budgets within each DM halo, we provide the most direct analysis of model outputs. However, we also note that uncertainties in the observational conversion of luminosity to stellar (and total baryonic) mass are systematically related to the spectral energy SED fitting methods used in order to extract physical quantities from the multiwavelength observations, and on the quality of the observations themselves, this is known to have large uncertainties and we hope in a subsequent work, to utilize synthetic spectra using the detailed star formation histories, galaxy geometries, gas and dust content, in order to self-consistently model the multiwavelength SED and make comparisons with the luminous properties of galaxies. In Fig. 4, we show the Schecter function fit to the Bell et al. (2003a) estimate for the local stellar mass function, in order to generate this mass function the authors utilize a large sample of galaxies from the Two Micron All Sky Survey (2MASS) and the Sloan Digital Sky Survey (SDSS) converting galaxy luminosity into stellar mass using simple models to convert the optical and near-infrared observations into stellar masses.

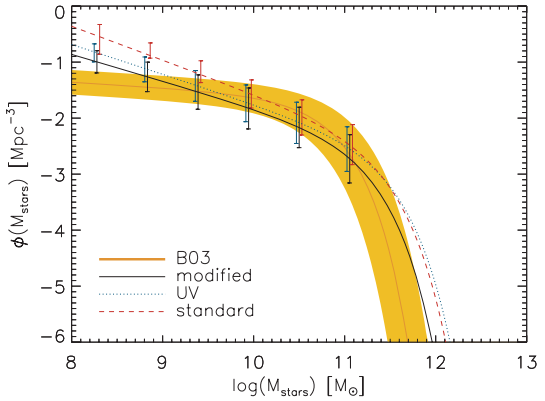


**Figure 4.** Stellar mass function output by each of our three model realizations compared with the Bell et al. (2003a) estimate. We find that the most sophisticated treatment of the baryonic physics results in agreement to the observations in all but the lowest mass haloes ($M_s < 10^9\,M_{\odot}$), where we find that we overproduce the stellar matter by approximately a factor 2. Note that, due to large uncertainties in observational mass-to-light ratios, we associate 0.3-dex errors in the stellar mass determinations, and 0.4-dex in the value of $\phi(M_{\rm stars})$, shown by the shaded area. Model error-bars represent Poissonian uncertainties due to the finite sample size of synthetic galaxies.

As we have shown in Fig. 4, using three levels of sophistication, we are able to highlight the differences between; a 'standard' model,

whereby we ignore the effects of a photoionizing background and employ a standard Schmidt–Kennicutt (Kennicutt 1998) star formation law, a 'UV' model whereby we include the suppression of mass flowing into galaxies through photoionization (see equations 6 and 7), and a 'sophisticated' model, which combines the effects of a photoionizing background with a two-phase ISM and modified star formation law. We will refer to these model names throughout the next sections.

More specifically, using a 'standard' model, we significantly overproduce the number density of low-mass galaxies. This occurs even when we increase supernovae feedback efficiencies to extremely high levels (see Mo et al. 2005 for a discussion), further pushing the parameter to higher values than $\epsilon_{\rm sn} = 0.7$ would result in largely unphysical models, and it is clear that reproducing observations using this basic framework does not occur naturally.[5] Secondly, increasing the supernovae feedback efficiencies whilst lowering the star formation efficiencies simply has the effect of reducing the stellar mass but not the gaseous mass, resulting in gas fractions which *increase* with increasing supernovae efficiency and thus are in disagreement with observations (see Mo et al. 2005 for a detailed discussion).

By suppressing the initial in-fall of material due to an ionizing UV background radiation, we are able to improve agreements with the mass function. However, we achieve the best reproduction of the stellar mass function through the additional reduction in star formation efficiency when employing the 'sophisticated' star formation law, which is determined by the amount of $H_2$ gas present in galaxy discs.

Alone, the stellar mass function provides a crucial observation for any physical galaxy formation model to reproduce, but by simultaneously comparing both the stellar and gaseous properties of galaxies, we are able to break degeneracies between gas infall and cooling, star formation and feedback processes, resulting in a significantly improved constraint on the theoretical framework. This has led previous authors to claim that the standard model, whereby low-mass systems support efficient gas cooling leading to large gaseous rotationally supported discs, which then undergo mild star formation, significantly overpredicts galaxy H I masses when compared to observations (see Mo et al. 2005) causing serious tension between theory and observation.

In Fig. 5, we compare model results with the Bell et al. (2003b) baryon mass function. We find that suppressing the infall of baryonic gas due to an ionizing UV background significantly improves agreement between observation and model output, since material is prevented from in-falling into the haloes initially and thus requiring less feedback in order to gain agreement of the low stellar and gas fractions in these haloes. A final and further improvement between model and observation is achieved by partitioning the ISM into neutral and molecular gas, which has the effect of reducing the SFR efficiency preferentially in the lowest mass DM haloes. We find that the best agreement between model and observation naturally results from using the most sophisticated treatment of the ISM physics, and the initial infall of gas. We do, however, still find discrepancies in the lowest mass haloes [$M_{\rm star}(z = 0) < 10^9$], over-

[5] We note also that we use a universal stellar initial mass function (IMF) which has been constrained in order to reproduce the chemical properties of galaxies accurately, increased supernovae rates are achievable using a more top-heavy IMF, however this has a strong chance to offset other properties of the formed galaxies with respect to observations (see Romano et al. 2005 for a discussion.)

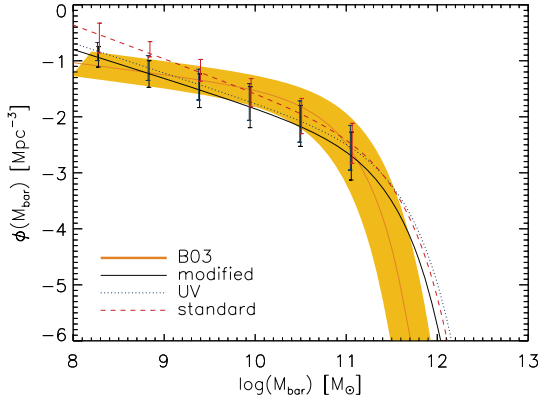


**Figure 5.** Baryonic mass function output by our three model realizations as compared to the Bell et al. (2003b) estimates. As is shown, the 'standard' approach over predicts significantly the amount of baryonic material at all masses, whereas adding the effects of a UV background and then a two-phase ISM results in progressive improvements. The most sophisticated realization results in a good fit to the observational mass function across all observable masses. Note that the shaded area represents the $1\sigma$ errors, discussed in Fig. 4. Model error-bars represent Poissonian uncertainties due to the finite sample size of synthetic galaxies.

predicting the baryon and stellar content within these DM haloes, and slightly overproducing the number density of the most massive galaxies. This issue is discussed in Section 5.

However, the observations (with their large uncertainties) remain relatively insensitive to the detailed properties of the galaxies at different masses, a strong motivation for the method adopted in Section 3, whereby linear scales amplify the discrepancies between models.

### 4.3 H I and $H_2$ mass functions

Due to the implemented star formation law within the 'sophisticated' model, whereby we partition the total cold gas mass into atomic and molecular hydrogen,[6] where $f_{\rm mol} = R_{\rm mol/(R_{mol}+1)}$, and $R_{\rm mol}$ is given by equation (40) at each time-increment in order to self-consistently generate a two phase ISM, we are able to make simultaneous predictions for both the H I and $H_2$ mass functions. In Fig. 6, we compare our model results to the observational estimates of Zwaan et al. (2005). The sample, comprising of 4315 extragalactic emission line estimated H I masses from the HIPASS catalogue, is complete down to $M_{H\rm I} \approx 10^8\,{\rm M}_\odot$, which allows for an unprecedented determination of the low mass slope. We find that above $M_{H\rm I} \approx 10^9\,{\rm M}_\odot$, we accurately reproduce the form and normalization of the mass function, but we do significantly overproduce the H I masses at the low-mass extreme.

Secondly, in Fig. 7, we compare the $H_2$ mass function as derived from the CO-mass function determination by Keres, Yun & Young (2003) based on the Five College Radio Astronomy Observatory extragalactic CO survey of 200 galaxies (Young et al. 1995). The conversion from CO to $H_2$ is achieved through a '$\chi$-factor' which proves to be a delicate and difficult task to determine, we utilize the $H_2$ mass function derived by Obreschkow & Rawlings (2009) as this appears to be the most robust determination, and also plot the $H_2$ mass function derived within the original Keres et al. (2005) work (using a constant $\chi$-factor). We refer the reader to their work for further details. We find that within observational errors, we

[6] Taking $M_{\rm H_2} = f_{\rm mol} M_{\rm hydrogen}$ and $M_{H\rm I} = (1 - f_{\rm mol}) M_{\rm hydrogen}$.

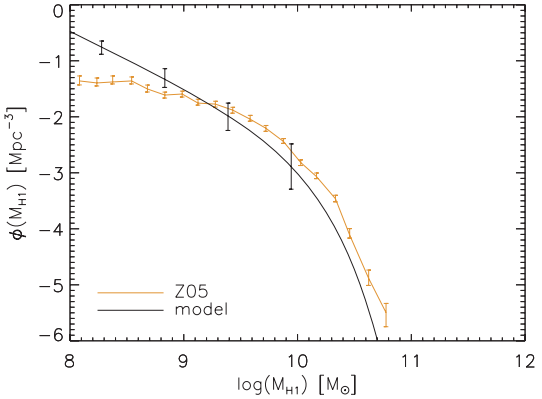


**Figure 6.** The H I mass function produced by our model as compared to the Zwaan et al. (2005) HIPASS galaxy sample. Using the combined effects of a UV background photoionizing radiation and a two-phase ISM we suppress the formation of low-mass systems. We find that we reproduce both the normalization and high mass cut-off accurately, but still slightly overproduce the number systems with $M_{\rm HI} < 10^9\,{\rm M}_\odot$, a minor effect discussed in Sections 4 and 5. Observational error bars are associated to $1\sigma$ uncertainties in determination of H I masses. Model error bars represent Poissonian uncertainties due to the finite sample size of synthetic galaxies.

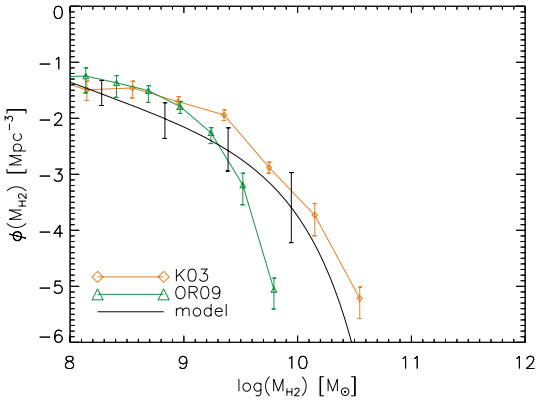


**Figure 7.** The $H_2$ mass function produced by our model as compared to the estimations by Keres et al. (2003). We find that we reproduce both the normalization, low and high mass cut-off within the observational range. Observational error bars are associated to $1\sigma$ uncertainties in determination of H I masses. Model error bars represent Poissonian uncertainties due to the finite sample size of synthetic galaxies.

reproduce this function over the entire observational range, however, we note that the large uncertainties within the determination of the precise value of the $\chi$-factor means that we are relatively loosely constrained, and we view this result as a general prediction of our model, rather than a constrained observational match.

Physically interpreting these results, we may conclude that utilizing a two-phase ISM whereby star formation scales only indirectly with the total gas mass, but directly with the molecular $H_2$ mass, we find that we may accurately reproduce both the H I and $H_2$ mass functions of galaxies apart from an overprediction of neutral H I within the lowest mass haloes. This discrepancy also appears within the stellar mass function (Fig. 4) and the baryonic mass function (Fig. 5), although it is greatly improved using the 'sophisticated' ISM treatment.

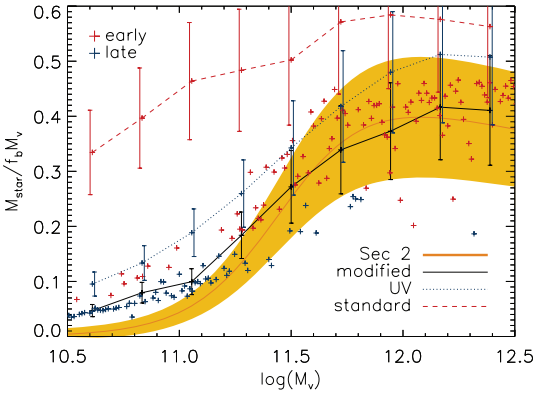


**Figure 8.** Deriving the relationships in Section 3, we show the baryon budget in the form of stellar material in DM haloes of different mass. Only by exploiting the effects of a UV background and a two-phase ISM can we reproduce the global form of this relationship, finding good agreements to observations at all masses, with a slight overprediction only in the lowest mass haloes. As can be seen, 'standard' approaches significantly overproduce stellar material on all mass ranges, but the discrepancy is clearest in the low-mass systems. The shaded region represents the $1\sigma$ observational uncertainty. Model error bars represent Poissonian uncertainties due to the finite sample size of synthetic galaxies.

### 4.4 Stellar-to-DM properties

Exploiting the methods outlined in Section 3, we are able to make observational mappings between DM halo masses and their contained stellar mass. In Fig. 8, we show the relative efficiency of conversion of baryonic material into stellar mass within DM haloes relative to the cosmological baryon to DM ratio $f_{\rm b} = \Omega_{\rm b}/\Omega_{\rm m} = 0.16$. These relationships provide direct observational constraints on to galaxy formation models and allow for a direct analysis of the relevant processes occurring over a range of mass scales (see Shankar et al. 2006). As can be seen, the lowest mass systems $[\log(M_v/{\rm M}_\odot) < 11]$ are strongly DM dominated, due to the inefficiency of weak gravitational potentials in these systems being able to capture and contain baryonic material and then efficiently form stars. Typically, these systems are strongly disc-dominated, late-type galaxies.

Intermediate mass systems $[11 < \log(M_v/{\rm M}_\odot) < 12]$ generally contain a range of morphological types with significant spheroid and disc components. The stellar content in these systems is a strong function of the mass, whereby the larger systems become richer in stellar mass fraction reaching a 'peak' ratio of stellar to DM where there is a minimum efficiency in the combined effects of supernovae and nuclear feedback processes. When we approach the highest mass DM haloes $[\log(M_v/{\rm M}_\odot) > 12]$, feedback through nuclear activity generated by an accreting SMBH is able to effectively remove the material. This effect becomes stronger in the higher mass systems and thus causes the flattening and slight downturn of the stellar conversion efficiency.

Overplotting model outputs using the 'standard', 'UV' and 'sophisticated' models, we may easily differentiate between outcomes due to the increased sensitivity of the plotting ranges. We see that the models which include the effects of a UV background show significant improvements over the entire mass range, and using the two-phase ISM physics and adopting the SFR dependent on $H_2$ mass, we are able to reproduce the observations to a high accuracy throughout the entire mass range due to the relative decrease in SF efficiency, with the only discrepancies at the lowest masses. It is important to

note here that due to the sequential build-up of matter within haloes from high redshifts to low, the importance of ionizing backgrounds and star formation on low-mass systems manifests throughout the entire mass range at $z = 0$ (see Somerville et al. 2008 for further discussion of this). Under the standard ΛCDM scenario, whereby small structures collapse first and form progressively larger systems, large structures at $z = 0$ are therefore significantly influenced by small scale processes at higher redshifts, where their constituent parts were forming and evolving, thus the low-mass behaviour is of global importance to galaxy formation theory.

### 4.5 Gas-to-DM properties

In analogy to the previous section, in Fig. 9, we plot the fraction of H I to DM halo mass, we are able to see that the gas fractions are highly sensitive to the different physical prescriptions, the scatter is attributed to the fact that the cold gas (and thus H I mass) component at any time is controlled by the competing processes of infall, star formation, feedback and recycling. We also find that, due to the uncertainties and intrinsic dispersion in the relationship between the DM and gaseous matter, the observational trend is not as constrained for the gaseous as for the stellar component. Observationally, the lowest mass DM haloes become progressively more depleted in H I, due to suppression of infall and increased efficiency in generating gaseous outflows, intermediate-mass DM haloes $11 > (\log(M_v/\mathrm{M}_\odot) > 11.5)$ possess the most H I mass, due to the global maxima in trapping and containing baryonic material in DM haloes (or conversely, a global minima in feedback processes), and at high masses we see a progressive loss of H I abundance in haloes, signifying an increase in removal of gaseous material through cooling inefficiencies and nuclear feedback processes.

In Fig. 9, we show the outputs for each of the three realizations, as can be clearly seen, the only successful reproduction of the majority of the observations is the 'sophisticated' model, whereby we model both the effects of a two-phase ISM and of an ionizing background radiation. Therefore, modelling the SFR depending linearly on the surface density of molecular gas in the disc component results in a correct conversion of cold gas to stellar material (as can be seen from simultaneous fits to both Figs 8 and 9), using the standard Schmidt–Kennicutt (Kennicutt 1998) star formation law (and their constrained normalization), we convert too much material from gas into stars, resulting in an overproduction of stellar mass and an underproduction of gas mass in all DM haloes, whereas the modification outlined in Dutton & van den Bosch (2009) allows for the correct fraction of virial mass in the H I phase, apart from in the lowest mass systems $[11 > (\log(M_v/\mathrm{M}_\odot)]$, where we find observation and model predictions in alarming disagreement.

As with previous works, but to a lesser extent, we find that we overproduce the amount of gas in the lowest mass DM haloes, and more worryingly, we do not reproduce the observed down-turn in gaseous mass within the lowest mass systems $[\log(M_v/\mathrm{M}_\odot) < 11]$. This mismatch clearly suggests that despite our suppression of baryonic material on to low-mass DM haloes, and improved star formation prescriptions we are still missing extra factors which dominate at $M_v(z = 0) < 10^{11}\,\mathrm{M}_\odot$. We may attribute this effect with our lack of description of environmental effects, since the lowest mass haloes are more probable to be located within larger overdensities and therefore subject to external forces (see the Section 5 and Mo et al. 2005 for more details).

### 4.6 Stellar-to-gas properties

It is suspected that within the lowest mass systems, gas collapse, star formation and supernovae feedback result in a self-regulated conversion of gas into stars, thus these effects can be seen to produce precisely the correct fraction of stars to gas in Fig. 10. Within our model the cold gas component fluctuates more than any other galaxy component since it is constantly being replenished due to infall and stellar recycling, exhausted through star formation and expelled through feedback processes. Therefore, directly comparing each galaxies gaseous and stellar properties provides a stringent comparison between observation and model. Interestingly, we find that plotting these quantities; we reproduce a tight correlation with relatively little scatter.

We find an overall agreement to the data across the entire mass range under investigation using the 'sophisticated' model, showing that the H I fraction becomes increasingly large with decreasing stellar mass, having roughly equal stellar and H I masses at

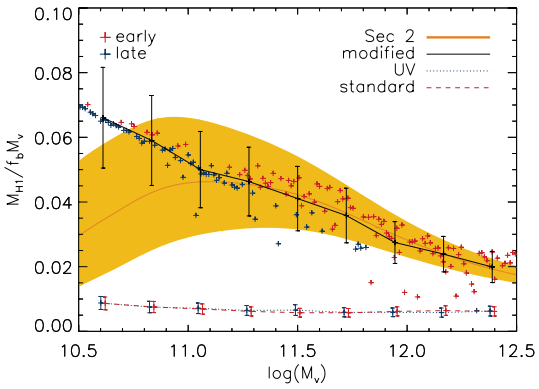


**Figure 9.** The fraction of baryonic matter in the form of H I relative to the cosmological fraction showing that using the 'sophisticated' model. We are able to successfully reproduce the derived relationships in Section 3 accurately down to relatively low-halo masses, but overpredict the H I mass by a factor of 2 within the lowest mass haloes. We discuss the implications of this in Section 5. The shaded region represents the $1\sigma$ observational uncertainty. Model error bars represent Poissonian uncertainties due to the finite sample size of synthetic galaxies.

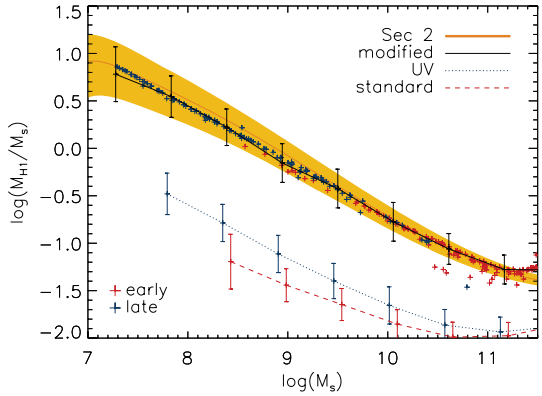


**Figure 10.** H I-to-stellar mass ratio as a function of the stellar mass. Using derived relationships from Section 3, we are able to assess the relationship between H I and stellar mass, finding that using a two-phase ISM and related SFR computations, we accurately reproduce the observations across the entire observational range, unlike the more simplistic frameworks, where we systematically convert too much cold gas into stellar material. The shaded region represents the $1\sigma$ observational uncertainty. Model error bars represent Poissonian uncertainties due to the finite sample size of synthetic galaxies.

$M_s \approx 10^9\,M_\odot$ increasing to a factor of ≈100 times more H I than stellar mass within systems with $M_s \approx 10^7\,M_\odot$. Conversely, without using the effects of a two-phase ISM and UV background radiation, we find a general offset in all masses, with an overefficient conversion of cold gas to stars (as may also be seen in Figs 8 and 9).

We also find that this result is relatively robust against parameter choices; only having a significant dependence on the star formation efficiency parameter (which is constrained observationally). We may attribute this to the fact that star formation is modelled as a function of the surface density of $H_2$ in galaxies and within the low-mass disc dominated systems is relatively inefficient (due to the low surface densities and relatively high star formation thresholds) resulting in a well-defined conversion of cold gas to stars and hence, H I to stellar mass ratio. This conclusion also has important consequences when considering the overproduction of both stellar and H I masses in the lowest mass DM haloes, since we accurately reproduce the self-regulation properties of galaxies (as the correct balance between star formation and feedback is required to simultaneously reproduce the correct gas and stellar mass budgets in DM haloes). Overproduction in the low-mass regions within Figs 8 and 9 therefore, must be attributed to the accretion of too much material, a conclusion which is confirmed by several other authors (see Mo et al. 2005 and references therein).

We would also like to plot the $H_2$ mass counterparts for Figs 8 and 9, however, due to the unconstrained mass functions, as discussed in Section 4.3, we are not able to construct conclusive observational constraints. Secondly, since partitioning the ISM within the single-phase ISM models is typically something relatively ad hoc, we do not perform this analysis here.

### 4.7 Star formation properties

A final useful diagnostic to be used to constrain galaxy formation models is the instantaneous SFR, which is found to vary significantly within galaxies of different stellar mass. In Fig. 11, we compare each model realization with the observational SFR estimates as a function of stellar mass by Elbaz et al. (2007), who used a large sample of SDSS galaxies with spectroscopic data in order to accurately determine the SFR (see Brinchmann et al. 2004).

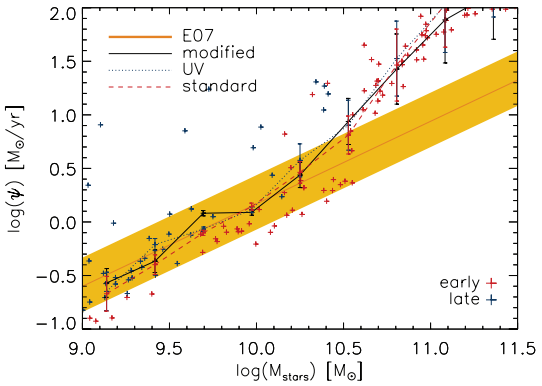


**Figure 11.** The predicted SFR as a function of the stellar mass at $z = 0$ for our three realizations compared to Elbaz et al. (2007). As can be seen, the SFRs in all three models are similar, all showing good agreements in the low-/intermediate-mass systems but models overpredicting the SFR in the highest mass systems. The shaded region represents the $1\sigma$ observational uncertainty. Model error-bars represent Poissonian uncertainties due to the finite sample size of synthetic galaxies.

We find little difference between the SFR predicted by each model realization as expected since each SFR prescription is constrained by $z = 0$ galaxy properties. Moreover, we generally find that within the low mass, disc-dominated region ($M_s < 10^{10}\,M_\odot$) we obtain a good agreement between model and observation, but significantly overpredict the SFRs in the largest galaxies. We may attribute this to a lack of active galactic nucleus (AGN) quenching within the disc component of the largest mass systems at late times, which has been applied in several models as a rather ad hoc 'radio-mode' feedback (see Bower et al. 2006; Croton et al. 2006). Since, within our models, we do not have any suppression of the growth of discs around large pre-formed bulges, aside from the late transition from the spheroid formation epoch to the disc formation epoch. We hope to investigate the effects of energetic feedback from a formed SMBH-spheroid system on the late properties of the disc since we hypothesize that; despite having a negligible effect on the growth of a pre-formed SMBH, star formation is prevented within the spheroid component at late times since even arbitrarily low accretion rates on to the central SMBH results in energetic feedback capable of heating the ISM, however, within our framework, during the quiescent disc growth phase no material is assumed to collapse on to the spheroid structure, even with a slight adjustment to our model we may allow for some material to collapse at late times on to the spheroid-SMBH system, resulting in the quenching of star formation in the larger systems and naturally generating Seyfert-type galaxies. However, for simplicity we have neglected this effect within this work, and hope to investigate the physical mechanisms capable of generating this self-consistently, within a subsequent work.

### 4.8 Two component ISM properties

As a main advance of this model over current SAMs, we detail the properties of the ISM by modelling the formation of molecular clouds ($H_2$ regions) through pressure arguments within the disc component. This enables us to modify the star formation law, and thus allows us to gain insights into the more detailed gas properties of normal galaxies under the semi-analytical framework.

Within this work, we highlight the importance of modelling the ISM in two-phases advocating it as a simple, yet important advance over current frameworks; whereby the formation of $H_2$ regions is determined by the planar pressure within the gaseous disc structure. This added ingredient is important for two main reasons. First, the decline in $H_2$ regions within low mass systems results in a higher fraction of cold gas in the form of neutral H I which is thus detectable through conventional 21-cm line surveys (see Barnes et al. 2001), whereas $H_2$ mass estimates prove to be significantly more difficult, relying on uncertain conversion factors between $H_2$ and CO-lines, therefore, assuming a single conversion between total cold gas and H I, as is commonly done in SAMs provides inaccurate outputs. Secondly, the star formation properties of galaxies have been shown to relate explicitly to the detailed properties of the internal structure of the ISM (see Krumholz, McKee & Tumlinson 2009; Gnedin, Tassis & Kravstov 2009; Obreschkow & Rawlings 2009), and therefore this added layer of complexity should now be embedded within current SAMs.

In Fig. 12, we show the fraction of cold gas which is in the form of $H_2$ within the disc component as a function of total stellar mass (disc and bulge masses). As can be seen, there is a tight relationship with little scatter in the lowest mass systems due to the overall dominance of disc components and the molecular fraction decreases steadily with decreasing stellar mass, we find a peak in molecular fraction corresponding to approximately 80 per cent

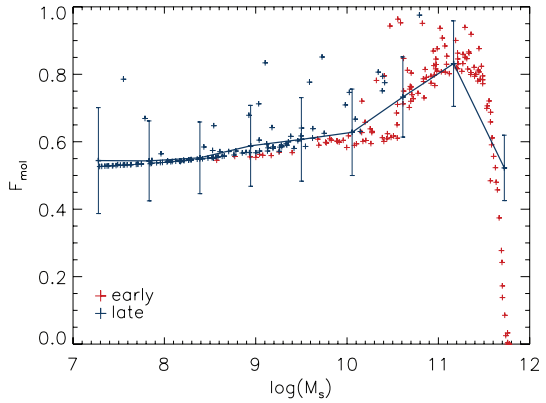


**Figure 12.** The molecular fraction of gas within galaxy discs. Showing that in low-surface density galaxies, the formation of molecular clouds is suppressed, and thus star-forming regions are diminished, and within the high-mass systems, the spheroid component dominates reducing the surface density in discs and therefore the molecular gas fraction rapidly declines. We hope to compare this result to observational studies as they become available. Model error-bars represent Poissonian uncertainties due to the finite sample size of synthetic galaxies.

$H_2$ at $M_s \approx 10^{11}\,M_\odot$ where the disc mass reaches a maximum. Above this mass, the spheroid component dominates and the disc surface density thus drops, lowering the efficiency of molecular cloud formation rapidly.

## 5 CONCLUSIONS

Prompted by several theoretical attempts to model the low-mass end of the stellar mass function (Somerville et al. 2008 and references therein) and significant observational effort to constrain the H I mass function using large surveys of galaxies (Barnes et al. 2001; Zwaan et al. 2005), within this work we have developed a physically motivated model in order to explain the inefficiencies of low-mass DM haloes in trapping baryonic material and forming stars. Motivated primarily by the importance of physical descriptions within small-scale systems which form the building blocks of larger systems within a hierarchically clustered Universe, also because theoretical models have either neglected or find significant troubles in simultaneously matching both the stellar and H I mass functions within the low mass end (see Mo et al. 2005).

Therefore, within this paper, we have utilized well-constrained observations of the stellar (Bell et al. 2003a,b) and H I (Zwaan et al. 2005) mass functions and a numerical technique (Shankar et al. 2006) which yield relationships between galaxy properties and their host DM haloes, as detailed by Evoli et al. (2009). Assuming a one-to-one mapping of these systems, we are thus able to make detailed comparisons between models and observations.

In order to interpret these phenomenological relationships physically, we develop a cosmologically grounded galaxy formation model outlined in C09, but with several significant modifications. Under this framework, we follow the development of baryonic material as it accumulates and evolves within growing DM haloes, and is subject to cooling, heating, possible angular momentum losses, star formation and recycling, and feedback through both supernovae events and the growth of a central SMBH. By comparing three model realizations with varying sophistication; one using a 'standard' approach, whereby the cosmological baryonic fraction $f_b = \Omega_b/\Omega_m$ is allowed to accrete within haloes throughout their lifetimes, and the star formation in discs (and thus the vast majority of low mass systems) is given by the Schmidt–Kennicutt (Kennicutt 1998) star formation law, determined by the total cold gas mass, a 'UV' model, whereby the infall of baryonic material within low-mass DM haloes is suppressed due to the presence of an ionizing UV background (see equations 6 and 7), and finally a 'sophisticated' model with a modified infall due to UV radiation and a modified star formation law which requires a two-phase ISM, comprising of neutral H I and molecular $H_2$ and typically results in a lower SFR within low-mass systems at early times.

These realizations clearly demonstrate that using a 'standard' approach, the most simple case is not able to simultaneously match both the stellar and H I mass functions, significantly overproducing low-mass galaxies (see Figs 4–6, 8 and 9), whereas the use of a 'sophisticated' approach, we are able to match observations reasonably accurately to relatively low masses, finding discrepancies within the lowest mass systems. As an additional consequence of the modified star formation law in the 'sophisticated' model realization, we naturally partition the cold gaseous ISM into H I and $H_2$ components, allowing for predictions of both of these quantities without the need for further assumptions, finding that we are able to match both components simultaneously to a good accuracy over the entire mass range when comparing to the $H_2$ results of Keres et al. (2003) and Obreschkow & Rawlings (2009) (Fig. 7), and only overproducing the amount of H I mass in the lowest mass galaxies (see Zwaan et al. 2005 and Fig. 6).

Finally, analysing several properties of galaxies against their stellar masses, we find that, unlike the simple approaches, the H I-to-stellar mass ratio is accurately reproduced using the sophisticated treatment (see Fig. 10), indicating that the self-regulation of star formation allows for the correct conversion of material, is relatively insensitive to the infall and supernovae feedback rates within physical limits. Comparisons of the SFRs within these models however show little difference at $z = 0$ as expected, and indicates a secondary problem with our simple physical model, overpredicting the SFR in the largest systems (with $M_v > 10^{11}\,M_\odot$), however, these systems are typically spheroid-dominated, and are therefore relatively insensitive to the details of the disc formation recipes.

It is clear to assess the limitations and the manifestations of this relatively simplistic approach to galaxy formation modelling. Under our improved framework, we still require large feedback efficiencies in order to sufficiently suppress star formation within the lowest mass systems: as has been studied by Mo et al. (2005), pre-heating through pre-virialized structure formation may further reduce the baryonic infall on to the lowest mass haloes, further reducing the need for such high SN efficiencies, other environmental effects such as tidal stripping and harassment may help to further improve the theoretical framework. However, despite these further degrees of freedom, we also note that changes in the initial mass function towards something more top-heavy will naturally have a higher supernovae fraction per stellar population, this therefore further reduces the need for highly efficient supernovae feedback within these models. In order to assess these additional effects, we would need to account for all the environmental effects associated with galaxy evolution, expanding our modelling from a single MAH to a full merger-tree framework, however, this adds a great deal more complication and uncertain physics (such as the evolution of satellite structures within DM haloes, the merger rates of galaxies, the outcome of galaxy components in mergers of different ratios), this will be the subject of a further analysis in a subsequent paper.

A second, minor shortcoming of our modelling appears to come from the complete separation of spheroid and disc growth within the two epochs of DM halo growth, whereby the disc and spheroid only share material through disc instabilities which are generally quite rare at late times due to the stabilization generated by the pre-formed spheroid. Despite showing that our quasi-monolithic scenario for the growth of galaxies to show promising results, we also hope to include explicitly the effects of merger events and environmental effects in a future work.

In conclusion, focusing mainly on the low-mass galaxy population, adopting several theoretical improvements over 'standard' SAMs, we are able to simultaneously match both the stellar, H I and $H_2$ mass budgets within DM haloes, and the star formation properties of galaxies within the observational ranges. This promising result indicates that at present, the 'standard' approach to modelling the low-mass evolution of galaxies is somewhat oversimplified within current SAMs which only have a single-phase ISM, and, due to the hierarchical nature of structure formation, may manifest as significant tensions in progressively larger systems within a full merger-driven framework (see Somerville et al. 2008 for a discussion). We therefore advocate the use of more sophisticated treatments of the ISM within current and future SAMs.

Assessing the limitations of our framework, we conclude that further suppression of infall on to the lowest mass systems would allow for a further reduction in the need for strong supernovae feedback and should further ease tensions between models and observations, this could only come through environmental effects such as tidal shocks or gravitational pre-heating (Mo et al. 2005), however, this effect has not been studied in detail through hydrodynamic simulations and remains to be fully investigated. By adding a channel whereby even small amounts of gaseous material may be transferred to the spheroid component during late times, small amounts of 'radio mode' AGN activity may be triggered, little affecting the spheroid or the SMBH masses, but significantly lowering the SFR in the discs, preferentially at large masses, naturally resulting in Seyfert-type active galaxies and reducing the SFR in these large discs, hopefully bringing Fig. 11 into better agreement with observations, we also hope to investigate the pan-redshift galaxy population under this framework (Cook et al. 2009b).

Interestingly, however, within this relatively simplistic framework we are able to self-consistently reproduce several of the key observations, it is therefore clear that mergers, to some degree, are not the dominant driver for the global evolution of the galaxy population. It will therefore provide a useful exercise to mount our physical prescriptions on to a full merger-tree DM background which should allow us to model environmental effects consistently. The main results from this paper indicate however, that using a relatively simple framework, we find a reasonable agreement to the stellar, H I and $H_2$ mass functions of galaxies arising naturally, thus, we advocate all current SAMs to begin to incorporate two-phase ISM physics into their frameworks.

## ACKNOWLEDGMENTS

We thank P. Salucci for providing the initial seeds for this work, and also to F. Shankar and A. Schurer for stimulating discussions which helped the progress of this work. MC thanks L. Paulatto for considerable computational assistance, and we thank A. Ferrara for critical reading of the manuscript. MC has been supported through a Marie Curie studentship for the Sixth Framework Research and Training Network MAGPOP, contract number MRTN-CT-2004-503929. EB acknowledges support from NSF Grant No. PHY-0603762. We thank the anonymous referee for useful comments which aided the clarity of this work.

## REFERENCES

Bardeen J. M., 1970, Nat, 226, 64
Barnes D. G. et al., 2001, MNRAS, 322, 486
Baugh C. M., 2006, Rep. Prog. Phys., 69, 3101
Bell E., McIntosh D. H., Katz N., Weinberg M. D., 2003a, ApJs, 149, 289
Bell E., McIntosh D. H., Katz N., Weinberg M. D., 2003b, ApJ, 585, 117
Benson A. J., Lacey C. G., Baugh C. M., Cole S., Frenk C. S., 2002, MNRAS, 333, 156
Benson A. J., Bower R. G., Frenk C. S., Lacey C. G., Baugh C. M., Cole S., 2003, ApJ, 599, 38
Blitz L., Rosolowski E., 2004, ApJ, 612, L29
Blitz L., Rosolowsky E., 2006, ApJ, 650, 933
Blumenthal G., Faber S. M., Flores R., Primack J. R., 1986, ApJ, 301, 27
Bower R. G., Benson A. J., Malbon R., Helly J. C., Frenk C. S., Baugh C. M., Cole S., Lacey C. G., 2006, MNRAS, 370, 645
Brinchmann J., Charlot S., White S. D. M., Tremonti C., Kauffmann G., Heckman T., Brinkmann J., 2004, MNRAS, 351, 1151
Bryan G. L., Norman M., 1998, ApJ, 495, 80
Bullock J. S., Kolatt T. S., Sigad Y., Somerville R. S., Kravtsov A. V., Klypin A. A., Primack J. R., Dekel A., 2001, MNRAS, 321, 559
Calura F., Pipino A., Matteucci F., 2008, A&A, 479, 669
Calzetti D. et al., 2007, ApJ, 666, 870
Cattaneo A., Dekel A., Devriendt J., Guiderdoni B., Blaizot J., 2006, MNRAS, 370, 1651
Christodoulou D. M., Shiosman I., Tohline J. E., 1995, ApJ, 443, 551
Cole S., Lacey C. G., 1996, MNRAS, 281, 716
Cook M., Lapi A., Granato G., 2009a, MNRAS, 397, 534 (C09)
Cook M., Barausse E., Evoli C., Lapi A., Granato G., 2009b, MNRAS, in press (arXiv:0910.3910)
Croton D. J. et al., 2006, MNRAS, 365, 11
Dekel A., Birnboim Y., 2008, MNRAS, 383, 119
Dekel A. et al., 2009, Nat, 457, 451
De Lucia G., Kauffmann G., White S. D. M., 2004, MNRAS, 349, 1101
Drapatz S., Zinnecker H., 1984, MNRAS, 210, 11
Driver S. P. et al., 2006, MNRAS, 368, 414
Dutton A., van den Bosch F. C., 2009, MNRAS, 396, 141
Elbaz D. et al., 2007, A&A, 468, 33
Evoli C., Salucci P., Cook M., 2009, in preparation
Gao Y., Solomon P. M., 2004, ApJ, 606, 271
Gil de Paz A. et al., 2007, ApJs, 173, 185
Gnedin O. Y., Kravtsov A. V., Klypin A. A., Nagai D., 2004, ApJ, 616, 16
Gnedin N. Y., Tassis K., Kravstov A. V., 2009, ApJ, 697, 55
Granato G. L. et al., 2000, ApJ, 542, 710
Granato G. L., De Zotti G., Silva L., Bressan A., Danese L., 2004, ApJ, 600, 580
Haiman Z., Ciotti L., Ostriker J. P., 2004, ApJ, 606, 763
Helfer T. T., Tnornley M. D., Regan M. W., Wong T., Sheth K., Vokel S. N., Blitz L., Bock D. C.-J., 2003, ApJS, 145, 259
Kauffmann G., White S. D. M., Guilderoni B., 1993, MNRAS, 264, 201
Kaufmann T., Bullock J. S., Maller A. H., Fang T., Wadsley J., 2009, MNRAS, 396, 191
Kawakatu N., Umemura M., Mori M., 2003, ApJ, 583, 85
Kennicutt R. C., 1998, ApJ, 498, 541
Kennicutt R. C. et al., 2003, PASP, 115, 928
Kennicutt R. C. et al., 2007, ApJ, 671, 333
Keres D., Yun M. S., Young J. S., 2003, ApJ, 582, 659
Keres D., Katz N., Weinberg D. H., Dave R., 2005, MNRAS, 363, 2
Kravtsov A. V., Gnedin O. Y., Klypin A. A., 2004, ApJ, 609, 482
Krumholz M. R., McKee C. F., 2005, ApJ, 630, 250
Krumholz M. R., McKee C. F., Tumlinson J., 2009, ApJ, 699, 850
Leroy A. K. et al., 2009, ApJ, 137, 4670
Li Y., Mo H.J., van den Bosch F.C., Lin W.P. 2007, MNRAS, 379, 689

Loveday J., 1998, in Thuan T. X. et al., eds, Proc. XVIII Moriond Astrophys. Meeting, Dwarf Galaxies and Cosmology. Editions Frontieres, Paris (astro-ph/9805255)
Lu Y., Mo H. J., Katz N., Weinberg M. D., 2006, MNRAS, 368, 1931
Macciò A. V. et al., 2007, MNRAS, 378, 55
Meyer M. J. et al., 2004, MNRAS, 350, 1195
Mo H. J., Mao S., 2004, MNRAS, 353, 829
Mo H. J., Mao S., White S. D. M., 1998, MNRAS, 295, 319
Mo H. J., Yang X., van den Bosch F. C., Katz N., 2005, MNRAS, 363, 1155
Nakamura O., Fukugita M., Yasuda N., Loveday J., Brinkmann J., Schneider D. P., Shimasaku K., Subbarao M., 2003, ApJ, 125, 1682
Navarro J. F., Steinmetz M., 2000, ApJ, 538, 477
Navarro J. F., Frenk C. S., White S. D. M., 1997, ApJ, 490, 493 (NFW)
Obreschkow D., Rawlings S., 2009, ApJ, 696, 129
Parkinson H., Cole S., Helly J., 2008, MNRAS, 383, 557
Romano D., Chiappini C., Matteucci F., Tosi M., 2005, A&A, 430, 491
Schurer A., Calura F., Silva L., Pipino A., Granato GL., Matteucci F., Maiolino R., 2009, MNRAS, 394, 2001
Shankar F., Lapi A., Salucci P., De Zotti G., Danese L., 2006, ApJ, 643, 14
Sheth R. K., Tormen G., 2002, MNRAS, 329, 61
Shen S., Mo H. J., White S. D. M., Blanton M. R., Kauffmann G., Voges W., Brinkmann J., Csabai I., 2003, MNRAS, 343, 978
Somerville R. S., Hopkins P. F., Cox T. J., Robertson B. E., Hernquist L., 2008, MNRAS, 391, 481
Spergel D. N. et al., 2007, ApJs, 170, 377
Springel V. et al., 2005, Nat, 435, 629
Sutherland R. S., Dopita M. A., 1993, ApJS, 88, 253
Toomre A., 1964, ApJ, 139, 1217
van den Bosch F. C., 2002, MNRAS, 332, 456
Walter F., Brinks E., de Blok W. J. G., Bigiel F., Kennicutt R. C., Thornley M. D., Leroy A., 2008, ApJ, 136, 2563
White S. D. M., Rees M. J., 1978, MNRAS, 183, 341
Wong T., Blitz L., 2002, ApJ, 569, 157
Wu J., Evans N. J., Gao Y., Solomon P. M., Shirley Y. L., Vanden Bout P. A., 2005, ApJ, 635, 173
Yang X., Mo H. J., van den Bosch F. C., 2003, MNRAS, 339, 1057
Young J. S. et al., 1995, ApJS, 98, 219
Zhao D. H., Mo H. J., Jing Y. P., Borner G., 2003, MNRAS, 339, 12 (Z03)
Zucca E. et al., 1997, A&A, 326, 477
Zwaan M. A., Meyer M. J., Staveley-Smith L., Webster R. L., 2005, MNRAS, 359, 30

This paper has been typeset from a TEX/LATEX file prepared by the author.